Applied Catalysis B: Environmental 162 (2015) 573–582

Contents lists available at ScienceDirect

Applied Catalysis B: Environmental

journal homepage: www.elsevier.com/locate/apcatb

PVP-stabilized nickel(0) nanoparticles as catalyst in hydrogen generation from the methanolysis of hydrazine borane or ammonia borane

Derya Özhava, Nihan Z. Kılıçaslan, Saim Özkar*

Department of Chemistry, Middle East Technical University, 06800 Ankara, Turkey

ARTICLE INFO

Article history:
Received 30 April 2014
Received in revised form 10 July 2014
Accepted 15 July 2014
Available online 22 July 2014

Keywords:
Hydrazine borane
Ammonia borane
Nickel nanoparticles
Hydrogen generation
Methanolysis

ABSTRACT

Herein we report the results of a detailed study on the *in-situ* generation of poly(N-vinyl-2-pyrrolidone) (PVP) stabilized nickel(0) nanoparticles and their catalytic activity in methanolysis of hydrazine borane and ammonia borane. PVP-stabilized nickel(0) nanoparticles with an average particle size of 3.0 ± 0.7 nm were *in-situ* generated from the reduction of nickel(II) 2-ethylhexanoate during the methanolysis of hydrazine borane in the presence of PVP at room temperature. Polymer stabilized nickel(0) nanoparticles could be isolated from the solution by centrifugation and characterized by UV–vis spectroscopy, XPS, TEM, and SAED. PVP-stabilized nickel(0) nanoparticles are highly active and long lived catalyst in hydrogen generation from the methanolysis of hydrazine borane and ammonia borane at ambient temperature. The results of kinetic study reveal that the methanolysis is first order with respect to catalyst concentration and zero order regarding to substrate concentration in both cases. PVP-stabilized nickel(0) nanoparticles provide 14,500 turnovers in hydrogen generation from the methanolysis of hydrazine borane and 5300 turnovers from the methanolysis of ammonia borane. They also provide an initial turnover frequency of 35.6 and 12.1 min^{-1} for the catalytic methanolysis of hydrazine borane and ammonia borane, respectively.

1. Introduction

The use of hydrogen as energy carrier is expected to facilitate the transition from the fossil fuels to the renewable energy sources, on the way towards a sustainable energy future [1,2]. However, the development of an efficient method for hydrogen storage is still the key issue in hydrogen economy [3]. Consequently, many efforts have been devoted to searching for chemical materials possessing high gravimetric hydrogen density suitable for both portable and stationary applications of hydrogen supply [4–6]. Among the several types of chemical hydrogen storage materials, boron-based hydrides have recently attracted great attention due to their high hydrogen content, safe storability, and easy H_2 release under mild conditions [7]. Ammonia borane (NH_3BH_3, AB) is a leading candidate as hydrogen storage medium because of its high potential capacity of 19.6 wt% H_2 [8], non-toxicity [9], and high stability in aqueous solution at room temperature [10]. Recently, another B-N compound, hydrazine borane ($N_2H_4BH_3$, HB; 15.4 wt% H) has been introduced as a promising chemical hydrogen storage material as well [11–13]. Hydrogen stored in AB and HB can be released *via* thermolysis [11,14], dehydrogenation in non-aqueous solvents [15,16] or solvolysis, such as hydrolysis or methanolysis [17–19]. Solvolysis is preferred because the other methods have harsh reaction conditions and slow hydrogen generation rate [20]. Transition metal(0) nanoparticles appear to be efficient catalysts in hydrogen generation from the hydrolysis of ammonia borane [21] and hydrazine borane [22–24]. The methanolysis of AB and HB can also release 3.0 equivalents of hydrogen in the presence of suitable catalyst.

Many different catalyst have been tested in the methanolysis of AB such as $RuCl_3$, $RhCl_3$, $PdCl_2$ [25], copper nanoparticles [26], polymer stabilized palladium(0) [27] and ruthenium(0) nanoparticles [28], Co-Co_2B, Ni-Ni_3B, Co-Ni-B nanocomposites [29], zeolite confined rhodium(0) nanoparticles [30], and MMT-immobilized ruthenium(0) nanoparticles [31]. Additionally, nickel(0) nanoparticles have been reported to catalyze the methanolysis of HB releasing 3.0 equivalents of H_2 [32].

$$NH_3BH_3 + 4CH_3OH \xrightarrow{catalyst} NH_4B(OCH_3)_4 + 3H_2 \quad (1)$$

$$N_2H_4BH_3 + 4CH_3OH \xrightarrow{catalyst} N_2H_5B(OCH_3)_4 + 3H_2 \quad (2)$$

* Corresponding author. Tel.: +90 312 210 3212; fax: +90 312 210 3200.
E-mail address: sozkar@metu.edu.tr (S. Özkar).

http://dx.doi.org/10.1016/j.apcatb.2014.07.033
0926-3373/

In the widely accepted method, the transition metal(0) nanoparticles are generated from the reduction of transition metal ions in solution in the presence of stabilizer or supporting materials [33]. Ideally, transition metal ions are reduced during dehydrogenation by the substrate when it is a strong reducing agent such as sodium borohydride [34]. It has been observed that ammonia borane is not able to reduce nickel(II) ions to nickel(0) nanoparticles in the catalytic hydrolysis of ammonia borane [35], with one exceptional case in which only 30% of nickel(II) chloride could be reduced by ammonia borane in aqueous solution without any stabilizing agent [36]. Therefore, the reduction of nickel(II) precursors has been achieved by using an additional stronger reducing agent, usually sodium borohydride. The addition of sodium borohydride causes complication in monitoring the hydrogen generated as it releases hydrogen as well. On the other hand, hydrazine borane, another potential hydrogen storage material, is able to reduce nickel(II) ions without additional reducing agent [19,32]. This difference in reducing ability of AB and HB implies that they should have different oxidation/reduction potential. Indeed we have recently shown that hydrazine borane has higher reducing ability than ammonia borane in methanol solution [37]. Herein, we report (i) the *in-situ* generation of nickel(0) nanoparticles stabilized by poly(N-vinyl-2-pyrrolidone) (PVP) from the reduction of nickel(II) ions by hydrazine borane in methanol solution, and (ii) their use as catalyst in hydrogen generation from the methanolysis of hydrazine borane and ammonia borane, separately. PVP-stabilized nickel(0) nanoparticles could be isolated from the reaction solution after the liberation of hydrogen from the methanolysis of HB and characterized by UV–vis electronic absorption spectroscopy, X-ray photoelectron spectroscopy (XPS), transmission electron microscopy (TEM), and selected area electron diffraction (SAED). The PVP-stabilized nickel(0) nanoparticles were found to be highly active catalyst in hydrogen generation from the methanolysis of HB and AB at ambient temperature. Kinetics of the catalytic methanolysis of HB and AB were studied depending on the substrate concentration, catalyst concentration and temperatures. Performing carbon disulfide poisoning experiments showed that PVP-stabilized nickel(0) nanoparticles are kinetically competent catalyst and the catalytic methanolysis of HB and AB is heterogeneous.

2. Experimental

2.1. Materials

Nickel(II) 2-ethylhexanoate solution (78 wt%) in 2-ethylhexanoic acid, sodium borohydride (99%), methanol (99%), tetrahydrofuran (99%), and ammonia borane (98%) were purchased from Sigma–Aldrich. Dihydrazine sulfate ($N_2H_4{\cdot}0.5H_2SO_4$) was purchased from Acros-Organics. Tetrahydrofuran and methanol were distilled over sodium/benzophenone and metallic magnesium, respectively and stored under argon. Distilled methanol was used in all methanolysis reactions under inert gas atmosphere unless otherwise specified. All glassware were cleaned with acetone, followed by copious rinsing with distilled water before drying in an oven at 120 °C.

2.2. Instrumentation

UV–vis electronic absorption spectra were recorded in methanol solution on Varian-Carry100 double beam instrument. The samples used for XPS analysis were harvested from *in-situ* generated PVP-stabilized nickel(0) nanoparticles solution at the end of the catalytic methanolysis of hydrazine borane. The polymer stabilized nanoparticles were seperated by centrifugation at 8000 rpm for 8 min and dried under vacuum. XPS analysis was performed on a Physical Electronics 5800 spectrometer equipped with a hemispherical analyzer and using monochromatic Al Kα radiation (1486.6 eV, the X-ray tube working at 15 kV, 350 W and pass energy of 23.5 keV). The transmission electron microscope (TEM) and selected area electron diffraction (SAED) images were taken on a JEM-2010 (JEOL) TEM instrument operating at 120 kV. The TEM samples were harvested from *in-situ* generated PVP-stabilized nickel(0) nanoparticles solution at the end of the catalytic methanolysis of hydrazine borane. The nanoparticle solution was centrifuged at 8000 rpm for 8 min. The separated nanoparticles were washed with ethanol to remove the excess PVP and other residuals. Then, the nanoparticles were redispersed in 5 mL acetone. One drop of the colloidal solution was deposited on carbon coated copper grid and evaporated under inert atmosphere. Samples were examined at magnifications between 150 and 600 K. Direct pyrolysis mass spectrometry, DP-MS, analyses were performed on a Waters Micromass Quattro Micro GC Mass Spectrometer with a mass range of 10–1500 Da and EI ion source, coupled to a direct insertion probe by recording the 70 eV EI mass spectra at a mass scan rate of 1 scan/s. NMR spectra were recorded on a Bruker Avance DPX 400 with an operating frequency of 128.15 MHz for ^{11}B. After the catalytic methanolysis of hydrazine borane or ammonia borane, a 0.1 mL aliquot of the reaction solution was transferred into quartz NMR tube containing 0.5 mL D-chloroform with a glass pipette.

2.3. Synthesis and characterization of hydrazine borane ($N_2H_4BH_3$)

Hydrazine borane ($N_2H_4BH_3$) was prepared and identified according to literature procedure [38]. The melting point of hydrazine borane: ~60 °C; (DP-MS) $m/z = 46$ (45.87 calculated for $N_2H_4BH_3$); ^1H NMR (400.1 MHz, CD_2Cl_2) 5.1 ppm (t, 2, NH_2–NH_2–BH_3), 3.4 ppm (b, 2, H_2N–NH_2–BH_3), 1.2 ppm (t, 3, H_2N–NH_2–BH_3); ^{11}B NMR (128.2 MHz, H_2O) −20 ppm (q, BH_3); ATR-IR (selected, cm^{-1}) 3310 (s), 3200 (s), 2840 (m), 2650 (m), 2370 (m), 2214 (m), 1620 (s), 1588 (m), 1435 (w), 1332 (m), 1150 (s), 910 (m), 747 (w) in agreement with the literature values [38].

2.4. In-situ generation of PVP-stabilized nickel(0) nanoparticles and catalytic methanolysis of hydrazine borane and ammonia borane

The *in-situ* generation of PVP-stabilized nickel(0) nanoparticles and concomitant methanolysis of hydrazine borane were performed in the same reaction flask. The catalytic activity of PVP-stabilized nickel(0) nanoparticles in the methanolysis of HB was determined by following the liberation of hydrogen gas. The experiment was performed as follows: The reaction flask with a stir bar is first evacuated to remove any trace of oxygen and water present and, then filled with nitrogen inert gas. The reaction flask is thermostated by circulating water through its jacket at 25 ± 0.5 °C or at a certain temperature specified. The gas outlet of the reaction flask is connected to a graduated glass tube filled with water through bubbler containing 20 mL of methylcyclohexane. A stock solution of 10 mM Ni^{2+} is prepared by transferring 0.115 mL (0.25 mmol Ni) nickel(II) 2-ethylhexanoate solution into 25 mL volumetric flask and diluting with methanol to 25 mL. The catalytic reaction solution with the desired concentration of nickel is prepared by taking certain aliquot from the stock solution and diluted by adding methanol. For instance, in order to prepare 1.0 mM Ni catalyst solution, a 1.0 mL (0.010 mmol Ni) aliquot of stock solution

is transferred into reaction flask containing 2.2 mg PVP (polymer to metal ratio of 2) and 6.0 mL methanol with a glass pipette. In a separate flask, 92 mg (1.8 mmol) HB is dissolved in 3 mL methanol while stirring under argon. Then, HB solution is added to the reaction flask *via* a gastight syringe, all at once, to launch catalytic methanolysis of HB. After an induction time the color changes from pale green to dark brown indicating the formation of nickel(0) nanoparticles in methanol solution and a rapid hydrogen generation from the methanolysis of HB starts immediately. The volume of hydrogen evolved during catalytic methanolysis is recorded by measuring the displacement of water level in the glass tube at constant pressure. When no more hydrogen liberated, experiment is stopped. An aliquot of the reaction solution is used for taking the ^{11}B NMR spectrum.

In catalytic methanolysis of ammonia borane, the same procedure as described above is followed. However, at this time preformed PVP-stabilized nickel(0) nanoparticles is used as catalyst in the methanolysis of AB because AB is not able to reduce nickel(II) ions to nickel(0) nanoparticles. For this purpose, after the liberation of expected amount hydrogen from the methanolysis of 180 mM HB catalyzed by PVP-stabilized nickel(0) nanoparticles, 64 mg (2.0 mmol) AB is added to the reaction flask making 200 mM AB solution. Due to the use of preformed PVP-stabilized nickel(0) nanoparticles, rapid hydrogen generation starts immediately without induction time after the addition of AB. The hydrogen generation from the methanolysis of AB is recorded by measuring the displacement of the water in glass tube at constant pressure. At the end of the methanolysis reaction, an aliquot of the reaction solution is used to take the ^{11}B NMR spectrum.

2.5. Kinetic studies for methanolysis of hydrazine borane and ammonia borane catalyzed by PVP-stabilized nickel(0) nanoparticles

In order to establish the rate law for methanolysis of hydrazine borane or ammonia borane catalyzed by PVP-stabilized nickel(0) nanoparticles, two different sets of experiments for each boron-based compounds were implemented as described in the previous section.

In the first set of the experiments, catalytic methanolysis of HB was started with 180 mM HB, nickel(II) 2-ethylhexanoate in various metal in the range of 1.0, 1.5, 1.75, 2.0 mM and 2.0 equivalent of PVP stabilizer per mole of nickel at $25 \pm 0.5\,^{\circ}$C. In the second set, methanolysis of HB in various substrate concentrations (180, 225, 270, 315 mM) was started with [PVP]/[Ni] of 2.0 and a catalyst concentration of 1.0 mM nickel at $25 \pm 0.5\,^{\circ}$C.

For catalytic methanolysis of AB, in the first set of the experiments, catalytic methanolysis of 200 mM AB was performed in the presence of preformed PVP-stabilized nickel(0) nanoparticles catalyst in various metal concentrations (0.5, 1.0, 1.5, and 2.0 mM Ni) at $25 \pm 0.5\,^{\circ}$C. In the second set of the experiments, a set of experiments were performed starting with different initial concentration of AB in the range 100–500 mM and keeping catalyst concentration constant at 1.0 mM Ni and [PVP]/[Ni] ratio constant at 2.0 at $25 \pm 0.5\,^{\circ}$C.

Finally, in order to determine the activation parameters for the catalytic reactions, methanolysis of 180 mM HB or 200 mM AB catalyzed by PVP-stabilized nickel(0) nanoparticles was performed at various temperatures in the range of 25–40 °C starting with catalyst concentration of [Ni] = 1.0 mM and the [PVP]/[Ni] ratio of 2.0. For each temperatures, the values of rate constants, k_{obs}, were determined and utilized to calculate activation energy (E_a) by using Arrhenius plots as well as enthalpy of activation ($\Delta H^{\neq}$) and entropy of activation ($\Delta S^{\neq}$) by drawing Eyring–Polanyi plots.

2.6. Determination of catalytic lifetime of PVP-stabilized nickel(0) nanoparticles in the methanolysis of hydrazine borane and ammonia borane

The lifetime of the catalyst was measured by determining the total turnover number (TTON) in the methanolysis of HB or AB catalyzed by PVP-stabilized nickel(0) nanoparticles. For this purpose, lifetime experiment was initiated by adding 0.50 mL (0.005 mmol Ni) aliquot from stock solution of nickel(II) 2-ethylhexanoate precursor by keeping [PVP]/[Ni] ratio of 2 and 450 mM HB or 500 mM AB at $25 \pm 0.5\,^{\circ}$C. When expected amount of hydrogen evolved, a new batch of substrate (HB or AB) was added to the reaction medium under nitrogen inert gas. Same procedure was applied until no more hydrogen liberation was observed.

2.7. Heterogeneity test for PVP-stabilized nickel(0) nanoparticles poisoned by carbon disulfide (CS_2) in the methanolysis of hydrazine borane

In order to confirm heterogeneity of PVP-stabilized nickel(0) nanoparticles, catalyst poisoning experiment was performed by using carbon disulfide (CS_2) as poison. Firstly, a 2.0 mM stock solution of CS_2 was prepared in 10 mL methanol. Then, a typical methanolysis reaction of HB catalyzed by PVP-stabilized nickel(0) nanoparticles was initiated with 1.0 mM (10 micromole Ni) nickel(II) 2-ethylhexanoate precursor and 180 mM HB at $25 \pm 0.5\,^{\circ}$C. At the time when about 40% of hydrogen evolved, 1.0 mL (2.0 micromole) CS_2 solution was added to reaction medium *via* a syringe in order to poison the catalyst. The hydrogen generation was observed to be ceased immediately upon addition of CS_2 into the reaction medium and no further hydrogen generation was monitored for 30 min.

3. Results and discussion

3.1. Preparation and characterization of PVP-stabilized nickel(0) nanoparticles

In-situ formation of nickel(0) nanoparticles from the reduction of nickel(II) ions by hydrazine borane in the presence of poly(N-vinyl-2-pyrrolidone) and concomitant hydrogen release from the methanolysis of hydrazine borane were achieved in the same medium. In a typical experiment, nickel(II) 2-ethylhexanoate and PVP were first stirred in methanol at 1000 rpm and, then, HB solution was injected to the reaction flask *via* a gastight syringe. When HB solution is added to the reaction solution containing nickel(II) ions plus PVP, both reduction of nickel(II) ions to nickel(0) and hydrogen liberation from the methanolysis of HB occur at the same time. The formation of nickel(0) nanoparticles from nickel(II) ions and concomitant hydrogen release from methanolysis of HB was followed by monitoring the volume of H_2 generated. Fig. 1 shows the plot of mol H_2 evolved per mol of HB *versus* time for the catalytic methanolysis of HB starting with 180 mM HB and 2.0 mM nickel(II) 2-ethylhexanoate plus 4.0 mM PVP in 10 mL methanol at $25 \pm 0.5\,^{\circ}$C. After an induction period of 15 min, the color of the solution changes from pale green to dark brown. Concomitantly, the hydrogen liberation starts immediately after the induction period and continues almost linearly until the complete consumption of HB. The sigmoidal shape of hydrogen generation curve and the color change indicate the reduction of nickel(II) ions and the formation of nickel(0) nanoparticles [39–41].

The reduction of nickel(II) ions to nickel(0) nanoparticles can also be followed in the UV–visible electronic absorption spectra taken from the reaction solution. Fig. 2 depicts the UV–visible electronic absorption spectra of nickel(II) 2-ethylhexanoate in

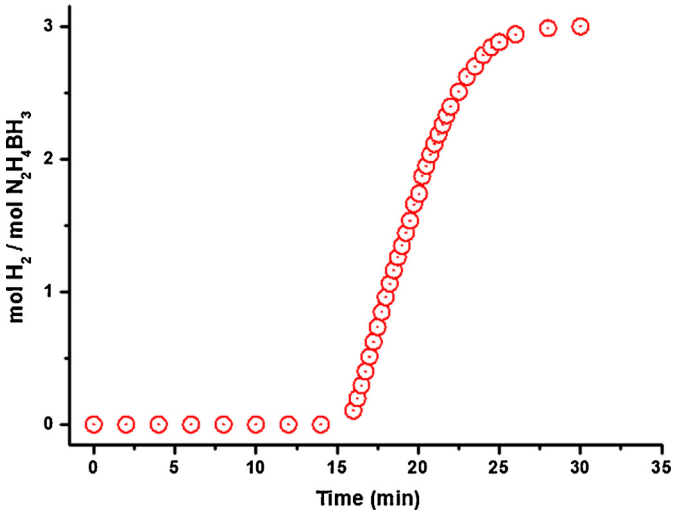

Fig. 1. Plot of mol of H_2 evolved per mol of hydrazine borane *versus* time for methanolysis of 180 mM HB starting with 2.0 mM nickel(II) 2-ethylhexanoate and 4.0 mM PVP in 10 mL methanol at 25 ± 0.5 °C.

methanol solution, nickel(II) 2-ethylhexanoate plus PVP before methanolysis and PVP-stabilized nickel(0) nanoparticles formed during the methanolysis of HB, all in 2.0 mM Ni solution. The UV–visible electronic absorption spectra of nickel(II) 2-ethylhexanoate in the absence or presence of PVP stabilizer show two relatively intense absorption bands at 301 and 400 nm plus a broad absorption band spanning from 600 and 800 nm [42,43]. Upon reduction of nickel(II) ions, these bands were replaced by a typical Mie exponential decay for the PVP-stabilized nickel(0) nanoparticles [44]. This spectroscopic observation indicates that the reduction of nickel(II) ions to nickel(0) nanoparticles is completed within 15 min.

The nickel(0) nanoparticles, formed *in-situ* from the reduction of nickel(II) ions during the methanolysis of hydrazine borane and stabilized by PVP, could be isolated from the reaction solution by centrifugation and characterized by transmission electron microscopy (TEM) and X-ray photoelectron spectroscopy (XPS). The oxidation states of nickel and the surface composition of

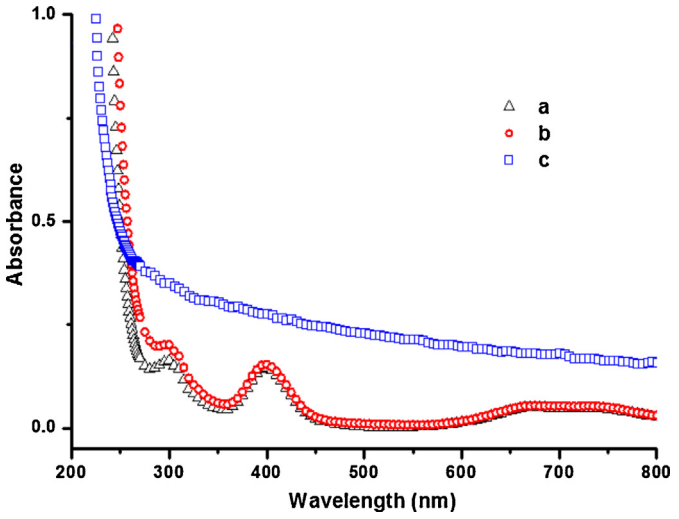

Fig. 2. UV–visible absorption spectra of (a) 2.0 mM nickel(II)-2-ethylhexanoate solution in methanol, (b) 2.0 mM nickel(II)-2-ethylhexanoate plus 4.0 mM PVP before methanolysis and (c) PVP-stabilized nickel(0) nanoparticles after methanolysis of 180 mM hydrazine borane with catalyst concentration at [Ni] = 2.0 mM plus 4.0 mM PVP.

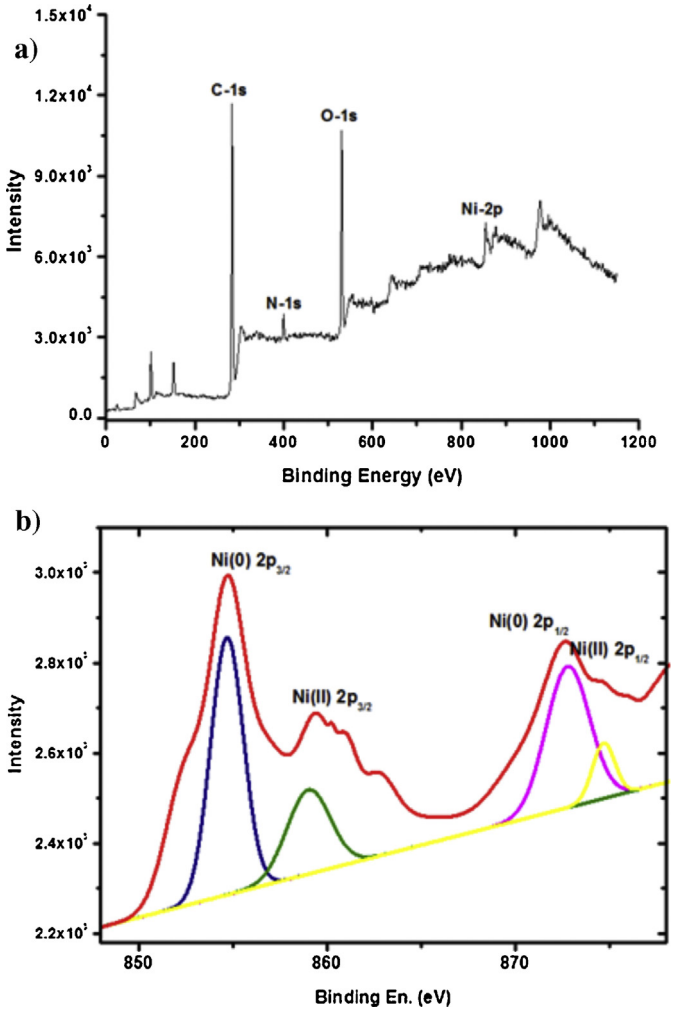

Fig. 3. (a) X-ray photoelectron (XPS) survey scan of PVP-stabilized nickel(0) nanoparticles. (b) XPS high resolution spectra of PVP-stabilized nickel(0) nanoparticles for Ni 2p after the methanolysis of hydrazine borane.

PVP-stabilized nickel(0) nanoparticles were examined by XPS. The survey-scan XPS spectrum of PVP-stabilized nickel(0) nanoparticles (Fig. 3a) indicates that nickel is the only element detected in the sample in addition to the elements of PVP (C, N, and O). Fig. 3b depicts a Ni 2p high resolution XPS spectrum of PVP-stabilized nickel(0) nanoparticles. Two prominent bands observed at 854.5 and 872.1 eV can be attributed to Ni(0) $2p_{3/2}$ and Ni(0) $2p_{1/2}$, respectively [45,46]. The relative intensities of the $2p_{3/2}$ and $2p_{1/2}$ are about 1:2. Compared to the values of bulk nickel, the $2p_{3/2}$ and $2p_{1/2}$ binding energies are slightly shifted to the higher values which can be attributed to the matrix effect [47] as well as quantum size effect [48]. Two additional lower intensity peaks still with relative intensity ratio 1:2 at higher energy 858.8 and 874.1 eV can be ascribed to Ni(II) $2p_{3/2}$ and Ni(II) $2p_{1/2}$, respectively [49,50]. By comparing to the spectral data for NiO [51], these bands indicate the presence of a small amount of NiO which can be formed as a thin oxide film on the surface of nickel(0) nanoparticles. Upon sputtering by argon ion bombardment, the intensity of former two bands of Ni(0) increases while the intensity of Ni(II) bands decreases relatively. This observation reinforces the assumption that NiO is formed on the surface of nanoparticles during XPS sampling when the nanoparticles are exposed to air for a few minutes.

The morphology and particle size distribution of PVP-stabilized nickel(0) nanoparticles were examined by transmission electron microscopy (TEM). TEM images depicted in Fig. 4a and b show that

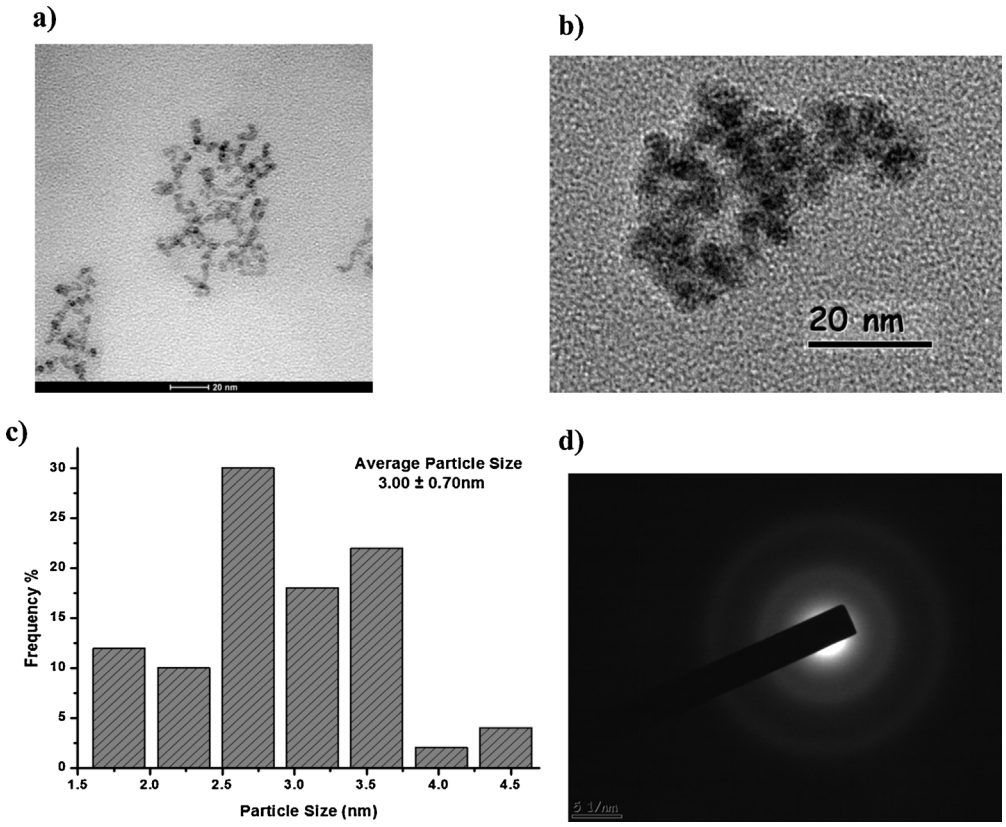

Fig. 4. (a and b) TEM images of PVP stabilized nickel(0) nanoparticles in different magnifications with scale bar of 20 nm, (c) the particle size histogram constructed by measuring the nanoparticles from different TEM images, (d) SAED ring pattern for the PVP stabilized nickel(0) nanoparticles showing the existence of fcc nickel.

PVP-stabilized nanoparticles are quite dispersed. By measuring the size of nanoparticles from different TEM images taken, a particle size histogram could be constructed (Fig. 4c) which gives an average particles size of 3.0 ± 0.7 nm for the PVP-stabilized nickel(0) nanoparticles. Selected-area electron diffraction (SAED) ring pattern of nickel(0) nanoparticles is given in Fig. 4d, which clearly shows the diffraction rings for nickel(0) metal with the face centered cubic (fcc) structure [52].

3.2. Catalytic activity of PVP-stabilized nickel(0) nanoparticles in the methanolysis of hydrazine borane or ammonia borane

PVP-stabilized nickel(0) nanoparticles, *in-situ* formed from the reduction of nickel(II) precursor by hydrazine borane, are highly active catalyst in hydrogen generation from the methanolysis of both amine boranes, HB and AB, even in low catalyst concentration and at room temperature.

3.3. Kinetics of methanolysis of hydrazine borane catalyzed by PVP-stabilized nickel(0) nanoparticles

Kinetics of the methanolysis of hydrazine borane in the presence of PVP-stabilized nickel(0) nanoparticles were studied in order to establish the rate law and determine activation parameters for the reaction. For this purpose, the first series of experiments were performed by varying the metal concentration and keeping the substrate concentration as well as the stabilizer to metal ratio constant. Fig. 5 illustrates the plots of mol H_2 evolved per mol of hydrazine borane *versus* time during the catalytic methanolysis starting with 180 mM HB, nickel(II) 2-ethylhexanoate in various metal concentration ([Ni] = 1.0, 1.5, 1.75, and 2.0 mM) and 2.0 equivalent of PVP stabilizer per mole of nickel at 25 ± 0.5 °C. In all of these experiments, hydrogen generation starts after an induction time that gets longer with the increasing nickel(II) concentration. Note that hydrazine borane acts as both reducing agent and substrate in catalytic methanolysis reaction. With the increasing nickel(II) concentration, [HB]/[Ni] ratio and, thus, the ratio of reducing agent to metal decreases leading to an extension of the time required for the reduction of nickel(II) to nickel(0). A rapid hydrogen generation starts immediately after the short induction period and continues almost linearly until the complete consumption of

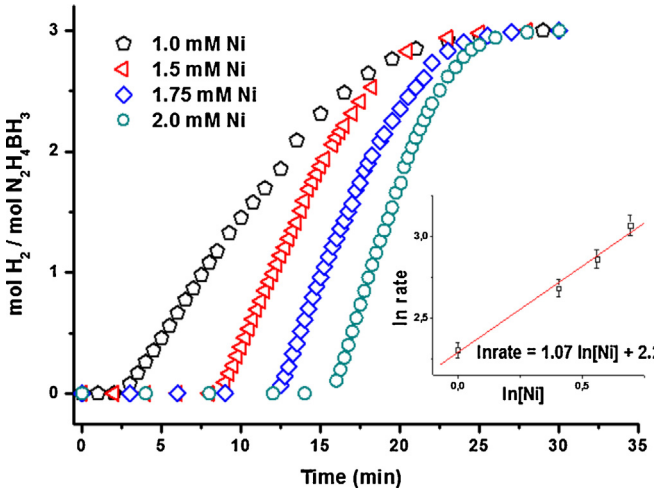

Fig. 5. Plots of mol H_2 evolved per mol of hydrazine borane *versus* time for methanolysis of 10 mL of 180 mM hydrazine borane in different metal concentrations ([Ni] = 1.0, 1.5, 1.75, and 2.0 mM) and 2.0 equivalent of PVP stabilizer per mole of nickel at 25.0 ± 0.5 °C. Inset: Plot of hydrogen generation rate *versus* the concentration of nickel (both in logaritmic scale).

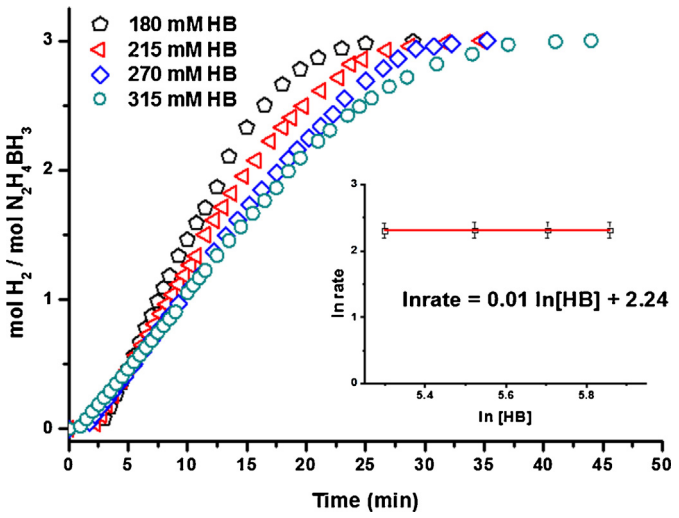

Fig. 6. Plots of mol H_2 evolved per mol of hydrazine borane *versus* time for the methanolysis of hydrazine borane in different substrate concentrations (180, 225, 270, 315 mM) starting with [PVP]/[Ni] of 2.0 and a catalyst concentration of 1.0 mM nickel at 25 ± 0.5 °C. Inset: Plot of hydrogen generation rate *versus* substrate concentration (both in logaritmic scale.).

hydrazine borane substrate. The hydrogen generation rate was determined from the linear portion of the graph for each experiment and plotted *versus* the initial concentration of nickel, both axes in logarithmic scale. This plot gives a straight line with a slope of 1.07 indicating that the methanolysis of hydrazine borane catalyzed by PVP-stabilized nickel(0) nanoparticles is first order with respect to catalyst concentration.

The effect of substrate concentration on the hydrogen generation rate was investigated by performing a series of experiments with various concentration of hydrazine borane and keeping the [PVP]/[Ni] ratio and catalyst concentration constant. The plots of mol H_2 evolved per mol of HB *versus* time are depicted in Fig. 6 for the methanolysis of HB in various substrate concentrations (180, 225, 270, 315 mM) starting with [PVP]/[Ni] of 2.0 and a catalyst concentration of 1.0 mM Ni at 25 ± 0.5 °C. In all of these experiments, a rapid hydrogen generation from methanolysis of hydrazine borane starts immediately after a very short induction time (less than 3 min) and continues linearly until the complete consumption of substrate. The hydrogen generation rate was determined from the linear portion of each plot for the methanolysis of HB performed starting with different substrate concentrations. The inset of Fig. 6 shows the plot of hydrogen generation rate *versus* substrate concentration, both in logarithmic scales, which gives a line with the slope of 0.01 ≈ 0 indicating that methanolysis of HB catalyzed by PVP-stabilized nickel(0) nanoparticles is zero order with respect to substrate concentration. It is noteworthy that as the substrate concentration increases from 180 to 315 mM, the hydrogen generation rate from the methanolysis of hydrazine borane decreases slightly from 94.6 to 56.6 mL min^{-1} g^{-1}. The small decrease in hydrogen generation rate can be ascribed to the increase in viscosity of reaction solution due to the increasing substrate concentration. A similar effect has been reported for hydrogen generation from the hydrolysis of sodium borohydride [53–55]. As the substrate concentration increases, the increasing viscosity of solution has been shown to inevitably retard the mass transfer and, thus, to reduce the solvolysis efficiency [56].

The rate law for the catalytic methanolysis of hydrazine borane can be established from the results of kinetic study (Eq. (3)).

$$\frac{-3d[N_2H_4BH_3]}{dt} = \frac{dH_2}{dt} = k[Ni] \quad (3)$$

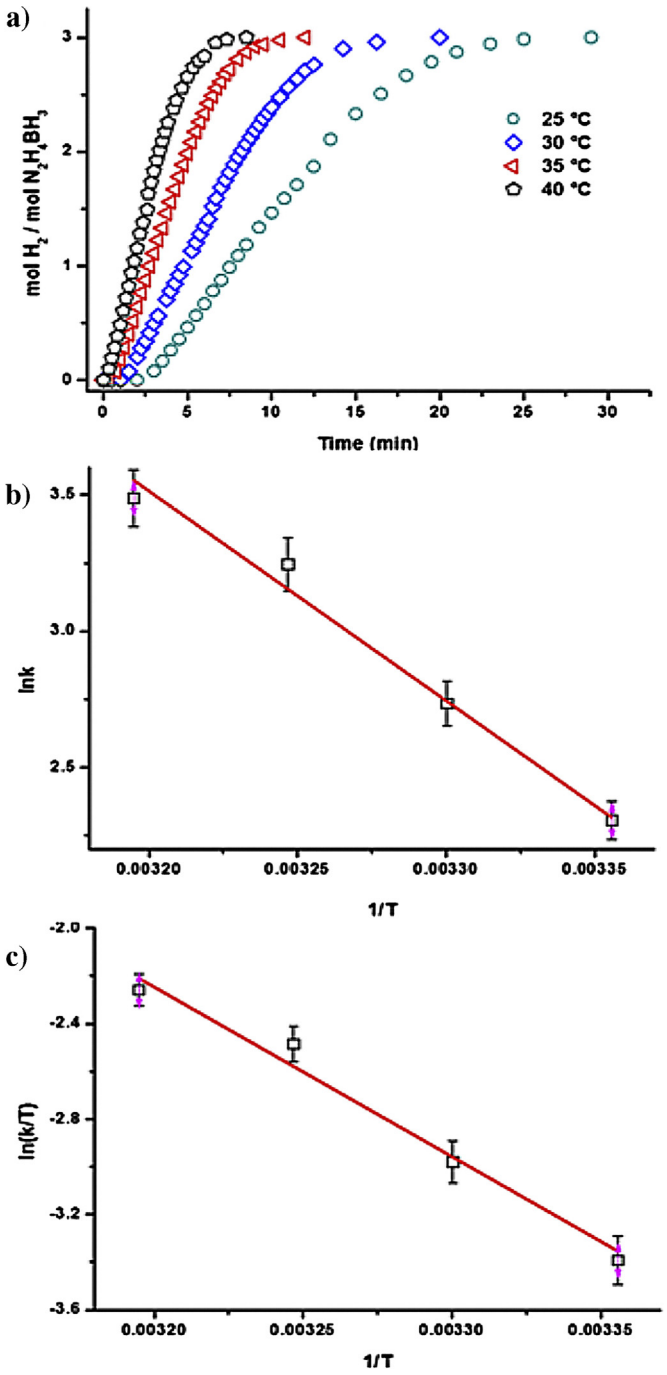

Fig. 7. (a) Plots of mole H_2 evolved per mole of hydrazine borane *versus* time for the catalytic methanolysis of hydrazine borane at various temperatures in the range of 25–40 °C keeping the concentration of substrate at [HB] = 180 mM and nickel at [Ni] = 1 mM as well as the [PVP]/[Ni] ratio at 2.0 constant. (b) Arrhenius plot, (c) Eyring plot.

Activation parameters for the methanolysis of hydrazine borane catalyzed by PVP-stabilized nickel(0) nanoparticles was obtained by performing a series of experiments at various temperatures in the range of 25–40 °C keeping the concentration of substrate at [HB] = 180 mM and catalyst at [Ni] = 1.0 mM as well as the [PVP]/[Ni] ratio at 2.0 constant. Fig. 7a shows the plots of mol H_2 evolved per mol of HB *versus* time for the catalytic methanolysis of hydrazine borane at different temperatures. As expected, the rate of hydrogen generation from the methanolysis of hydrazine borane increases with the increasing temperature. It is noteworthy that the

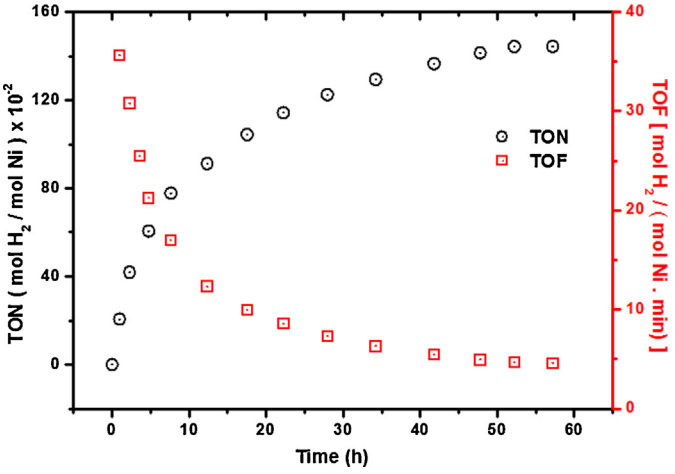

Fig. 8. Plot of total turnover number (TTO) or turnover frequency *versus* time for the methanolysis of hydrazine borane ($N_2H_4BH_3$) with 10 mL solution of nickel(II) 2-ethylhexanoate containing 0.5 mM Ni, 1.0 mM PVP and 450 mM HB (for each run) at 25 ± 0.5 °C.

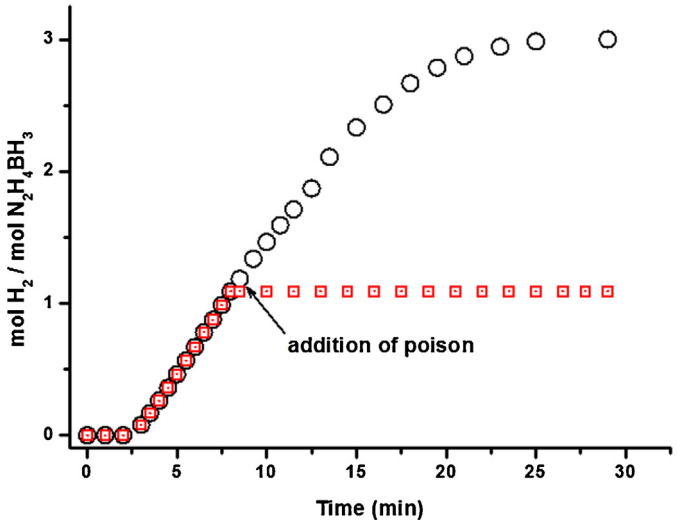

Fig. 9. Plots of mol H_2 evolved per mol of hydrazine borane *versus* time for the methanolysis of 180 mM hydrazine borane catalyzed by PVP-stabilized nickel(0) nanoparticles (1 mM Ni) with and without addition of 0.2 equiv. CS_2 at 25.0 ± 0.5 °C.

induction time also decreases with the increasing temperature because the reduction of nickel(II) ions by HB speeds up at higher temperatures, so the nucleation of nanoparticles. The observed rate constants (k_{obs}), determined from the linear part of each plot of mol H_2 evolved per mol of HB *versus* time for the catalytic methanolysis of HB at different temperatures, were used in the construction of Arrhenius and Eyring plots given in Fig. 7b and c, respectively. The apparent activation parameters were found by using Arrhenius [57] and Eyring [58] equations; the activation energy E_a^{app} = 63 ± 2 kJ/mol, the activation enthalpy $\Delta H^{\neq,app}$ = 61 ± 2 kJ/mol, and the activation entropy $\Delta S^{\neq,app}$ = −22 ± 4 J/mol K. The activation energy value obtained for the methanolysis of hydrazine borane catalyzed by PVP-stabilized nickel(0) nanoparticles is comparable to the reported E_a values for the same reaction using bulk nickel (E_a^{app} = 65 kJ/mol) [32], poly(4-styrenesulfonic acid-co-maleic acid) stabilized nickel(0) nanoparticles (E_a^{app} = 73 kJ/mol) [59], hydroxyapatite supported rhodium(0) nanoparticles (E_a^{app} = 65 kJ/mol) [22].

The catalytic lifetime of PVP-stabilized nickel(0) nanoparticles was measured by determining the total turnover number provided by the nanoparticles in the methanolysis of hydrazine borane at room temperature before their deactivation. Such a lifetime experiment was performed starting with 10 mL solution of nickel(II) 2-ethylhexanoate containing 0.5 mM Ni, 1.0 mM PVP and 450 mM HB at 25 ± 0.5 °C. When expected amount of H_2 gas evolved, a new batch of substrate was added to the reaction flask and hydrogen generation was monitored. This procedure was repeated until no more gas evolution was observed. As shown in Fig. 8, the *in-situ* generated PVP-stabilized nickel(0) nanoparticles provide 14,500 turnovers in hydrogen generation from the methanolysis of HB at 25 ± 0.5 °C before deactivation. The initial turnover frequency (TOF) value is 1850 h^{-1} for PVP-stabilized nickel(0) nanoparticles in hydrogen generation from methanolysis of hydrazine borane at 25 ± 0.5 °C. These TON and TOF values are comparable to those given in literature for the methanolysis of hydrazine borane catalyzed by bulk nickel without any stabilizer, TON = 11,200 and TOF = 1430 h^{-1} [32]. The higher TON and TOF value of PVP-stabilized nickel(0) nanoparticles than that of bulk nickel(0) can be ascribed to the smaller particle size due to the polymer stabilization, consequently the larger surface area [60]. In the absence of stabilizer, the nanoparticles tend to agglomerate ultimately to the bulk metal, which leads to a significant decrease in catalytic activity. When used in large amount the polymer will cover the whole surface of nanoparticles making them very stable against agglomeration, however with no catalytic activity as the surface atoms are not accessible any more. Therefore, the relative amount of stabilizer had to be optimized, such as in our case. In the earlier work no stabilizer has been used [32]. Note that chloride ion present in the solution is weakly coordinating, therefore, does not provide enough stabilization for the nickel nanoparticles [61]. In the absence of stabilizer, small nanoparticles formed are very active in the initial stage, however, as they agglomerate the catalytic activity decreases drastically. Therefore, nickel(0) nanoparticles in the absence of polymeric stabilizer are not long lived catalyst, providing 11,200 turnover over 17 h before deactivation. In the present work, the nickel(0) nanoparticles stabilized by PVP can provide 14,500 turnovers in hydrogen generation from the methanolysis of hydrazine borane at room temperature over 58 h before deactivation. Thus, PVP-stabilized nickel(0) nanoparticles have longer catalytic lifetime than the ones without PVP.

3.4. Carbon disulfide (CS_2) poisoning heterogeneity test for PVP-stabilized nickel(0) nanoparticles in the methanolysis of hydrazine borane

The heterogeneity of PVP-stabilized nickel(0) nanoparticles was investigated by performing CS_2 poisoning experiment. Due to the strong binding of poison to the metal center, the access of the substrate to the active site is blocked by poison [62,63]. In our poisoning experiment, after the liberation of 40% hydrogen from methanolysis of HB (180 mM) catalyzed by 1.0 mM Ni, when the catalytically active nickel(0) nanoparticles were certainly formed, 0.20 equiv. CS_2/mol of catalyst was injected to reaction flask, all at once; hereby, the activity of PVP-stabilized nickel(0) nanoparticles was inhibited and hydrogen generation from methanolysis of HB stopped immediately (Fig. 9). The complete cessation of catalytic methanolysis of HB upon addition of 0.2 equiv. CS_2 is a compelling evidence for the heterogeneity of PVP-stabilized nickel(0) nanoparticles in the methanolysis of HB.

3.5. Kinetics of methanolysis of ammonia borane catalyzed by preformed-PVP-stabilized nickel(0) nanoparticles

PVP-stabilized nickel(0) nanoparticles obtained at the end of hydrogen generation from the methanolysis of hydrazine borane were used as preformed catalyst in the methanolysis of ammonia borane. PVP-stabilized nickel(0) nanoparticles are also highly active

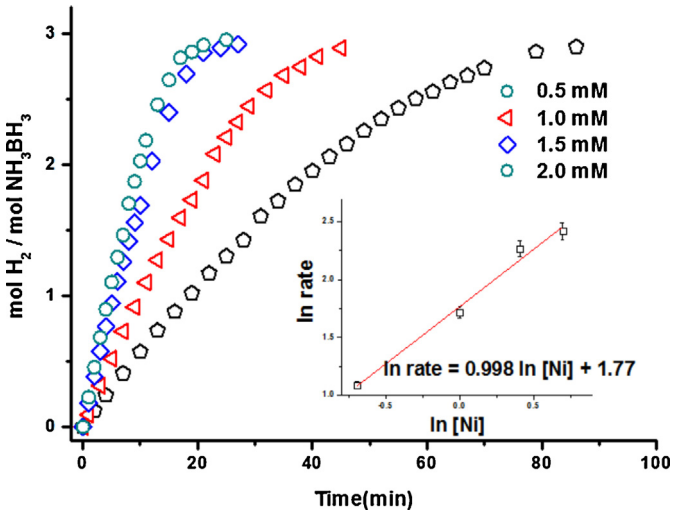

Fig. 10. Plots of mol H_2 evolved per mol of ammonia borane *versus* time for methanolysis of 200 mM ammonia borane in the presence of preformed PVP-stabilized nickel(0) nanoparticles catalyst in various metal concentrations ([Ni] = 0.5, 1.0, 1.5, and 2.0 mM) at 25.0 ± 0.5 °C. Inset: Plot of hydrogen generation rate *versus* the concentration of nickel (both in logaritmic scale.).

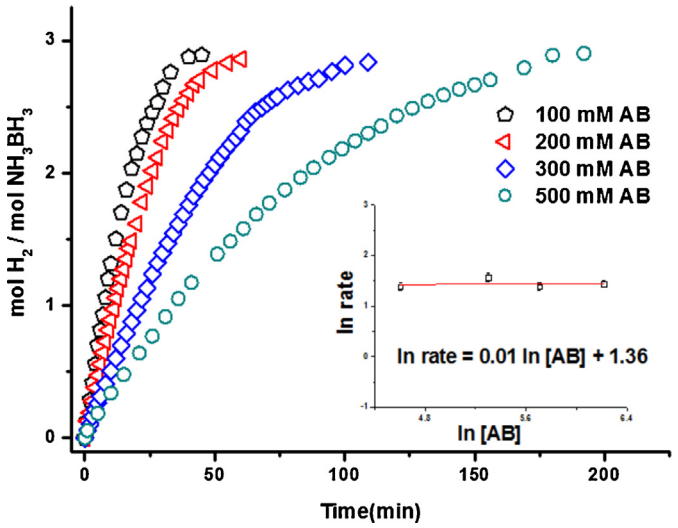

Fig. 11. Plots of mol H_2 evolved per mol of ammonia borane *versus* time for the methanolysis of ammonia borane in different concentrations (100, 200, 300, 500 mM) keeping catalyst concentration constant at 1.0 mM Ni and [PVP]/[Ni] ratio constant at 2.0. Inset: Plot of hydrogen generation rate *versus* substrate concentration (both in logaritmic scale.).

catalyst in hydrogen generation from the methanolysis of ammonia borane at low temperature. The kinetics of methanolysis of ammonia borane catalyzed by PVP-stabilized nickel(0) nanoparticles were studied depending on the concentration of substrate and catalyst as well as the temperature. Fig. 10 depicts the plot of mol H_2 evolved per mol of AB *versus* time during the catalytic methanolysis of 200 mM AB in the presence of preformed PVP-stabilized nickel(0) nanoparticles catalyst in various metal concentrations (0.5, 1.0, 1.5, and 2.0 mM Ni) at 25 ± 0.5 °C. Since a preformed catalyst is used in the methanolysis of ammonia borane, the hydrogen generation starts immediately without induction time even at high concentration of metal catalyst. The formation of nickel(0) nanoparticles during the methanolysis of hydrazine borane is accompanied by the generation of tetramethoxyborate ion as by-product, which might be thought to influence the catalytic activity in the methanolysis of ammonia borane. A closer look at the plot in Fig. 1 shows that the hydrogen generation rate doesn't change in the course of methanolysis of hydrazine borane even though tetramethoxyborate ion accumulates. Similarly, the hydrogen generation rate from the methanolysis of ammonia borane (Fig. 10) does not change significantly in the course of reaction, particularly in high concentration of substrate. Conclusively, it is fair to assume that the tetramethoxyborate ion produced from the methanolysis of hydrazine borane doesn't have a noticeable influence on the catalytic activity in the methanolysis of ammonia borane in the concentration range used in one single run of methanolysis. The hydrogen generation rate from the methanolysis of ammonia borane in different catalyst concentration was determined from the linear portions of each plot. The graph of hydrogen generation rate *versus* metal concentration, both in logarithmic scale, is given in the inset of Fig. 10. This plot gives a straight line with a slope of 0.998 ≈ 1, indicating that methanolysis of ammonia borane is first order with respect to catalyst concentration.

In order to investigate the effect of substrate concentration on the hydrogen generation rate from the catalytic methanolysis of ammonia borane, a set of experiments were performed starting with different initial concentration of AB in the range 100–500 mM and keeping catalyst concentration constant at 1.0 mM Ni and [PVP]/[Ni] ratio constant at 2.0. Fig. 11 demonstrates the plot of mole H_2 evolved per mole of AB *versus* time during the catalytic methanolysis of AB at different substrate concentrations (100, 200, 300, and 500 mM). In all experiment, a rapid hydrogen generation is observed without induction period. The hydrogen generation rate is determined from the linear portion of each plot and utilized to construct the plot of hydrogen generation rate *versus* AB concentration, both in logarithmic scale, as shown in the inset of Fig. 11. The slope of the line obtained is 0.01 ≈ 0 indicating that catalytic methanolysis of AB is zero order with respect to substrate concentration.

Rate law for the catalytic methanolysis of AB can be established from the results collected by the kinetic experiments (Eq. (4)).

$$\frac{-3d[NH_3BH_3]}{dt} = \frac{dH_2}{dt} = k[Ni] \quad (4)$$

To determine activation parameters for the methanolysis of ammonia borane catalyzed by preformed PVP-stabilized nickel(0) nanoparticles, a series of experiments were performed at various temperatures in the range 25–40 °C keeping the concentration of substrate at [AB] = 200 mM and nickel at [Ni] = 1.0 mM as well as the [PVP]/[Ni] ratio at 2.0 constant. Fig. 12 illustrates the plot of mol H_2 evolved per mol of AB *versus* time for the catalytic methanolysis of ammonia borane at different temperatures. As expected, the rate of hydrogen generation from the methanolysis of ammonia borane increases with increasing temperature. The observed rate constants for catalytic methanolysis of ammonia borane at various temperatures were calculated from the linear part of each plot given in Fig. 12a and used for the construction of Arrhenius and Eyring plots depicted in Fig. 12b and c, respectively, to determine the activation parameters: Arrhenius activation energy E_a^{app} = 62 ± 2 kJ/mol, activation enthalpy $\Delta H^{\neq,app}$ = 60 ± 2 kJ/mol, and activation entropy $\Delta S^{\neq,app}$ = −30 ± 2 J/mol.K. The activation energy calculated for the methanolysis of ammonia borane catalyzed by PVP-stabilized nickel(0) nanoparticles is larger than most of the literature values reported for the same reaction catalyzed by PVP-stabilized palladium(0) nanoparticles (E_a^{app} = 35 kJ/mol) [27], zeolite-confined rhodium(0) nanocluster (E_a^{app} = 40 ± 2 kJ/mol) [30], MMT-immobilized ruthenium(0) nanoparticles (E_a^{app} = 23.8 kJ/mol)[31] and carbon supported bimetallic $Co_{48}Pd_{52}$ nanoparticles (E_a^{app} = 25.5 kJ/mol) [18].

The catalytic lifetime of preformed PVP-stabilized nickel(0) nanoparticles was measured by determining the total turnover number provided by the nanoparticles in the methanolysis of

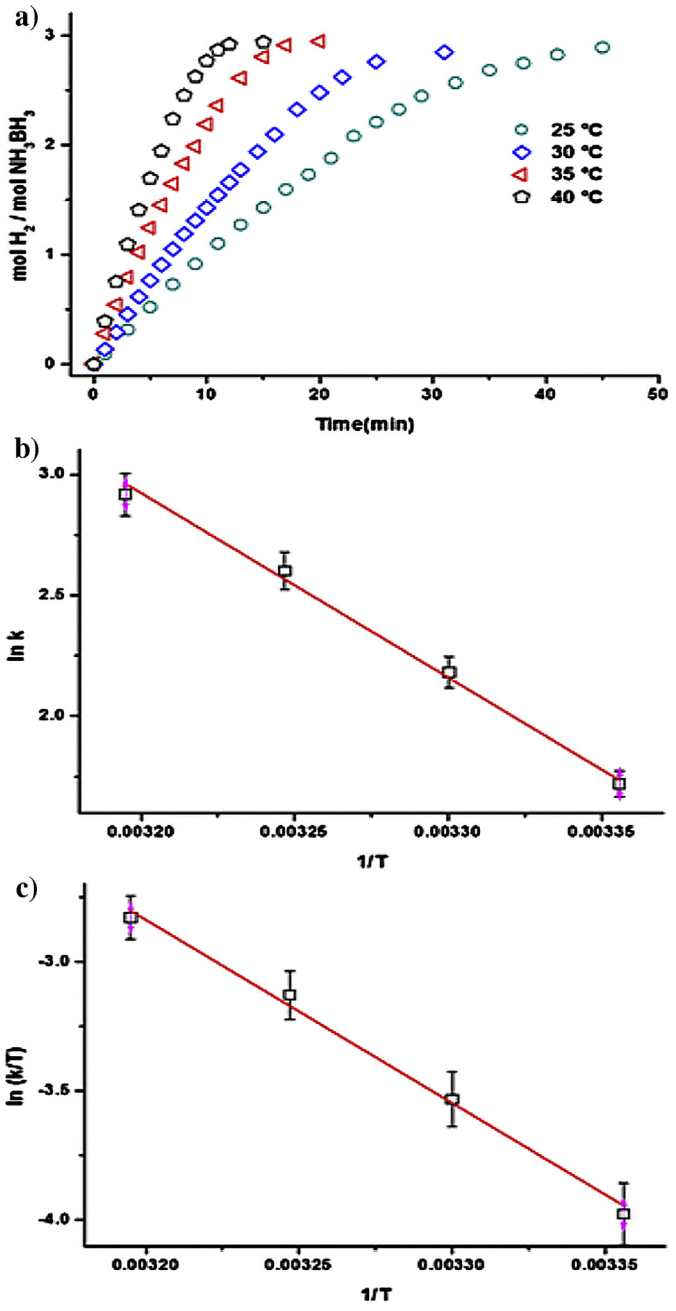

Fig. 12. (a) Plots of mol H_2 evolved per mol of ammonia borane *versus* time for the catalytic methanolysis of ammonia borane at various temperatures in the range 25–40 °C keeping the concentration of substrate at [AB] = 200 mM and nickel at [Ni] = 1 mM as well as the [PVP]/[Ni] ratio at 2.0 constant. (b) Arrhenius plot, (c) Eyring plot.

ammonia borane at room temperature before their deactivation. Such a lifetime experiment was started with 10 mL methanol solution of preformed PVP-stabilized nickel(0) nanoparticles containing 0.50 mM nickel catalyst, 1.0 mM PVP and 500 mM AB at 25 ± 0.5 °C. After the liberation of expected amount of H_2, a new batch of AB was added to the reaction flask and hydrogen generation was monitored. This procedure was followed until no more hydrogen evolved as the catalyst was deactivated. The preformed PVP-stabilized nickel(0) nanoparticles provide 5300 turnovers in hydrogen generation from methanolysis of AB at 25 ± 0.5 °C before deactivation (Fig. 13). The hydrogen generation rate slows down as the reaction proceeds and eventually ceases. This decrease in activity may be related to the deactivation effect of the boron

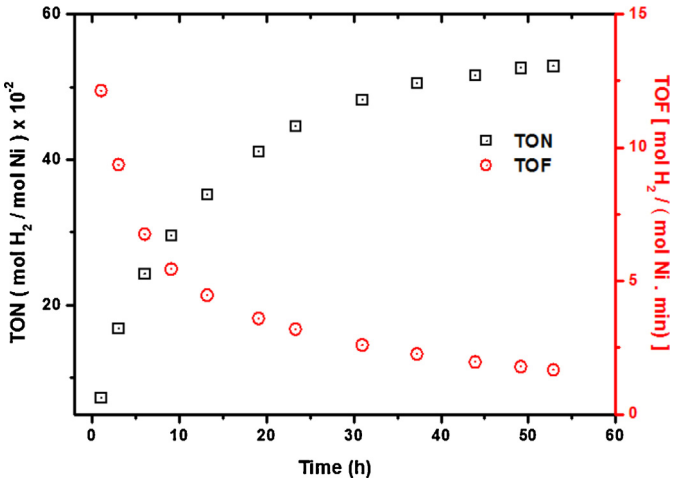

Fig. 13. Plot of total turnover number (TTO) or turnover frequency *versus* time for the methanolysis of ammonia borane (NH_3BH_3) with a 10 mL solution of preformed PVP-stabilized nickel(0) nanoparticles containing 0.5 mM Ni, 1.0 mM PVP and 500 mM AB (for each run) at 25 ± 0.5 °C.

containing by-products or increasing viscosity of solution. The initial turnover frequency (TOF) value is 12.1 min^{-1} (mol H_2/mol Ni min) for preformed PVP-stabilized nickel(0) nanoparticles in the catalytic methanolysis of AB at 25 ± 0.5 °C. It is noteworthy that preformed PVP-stabilized nickel(0) nanoparticles ensure the highest TOF value ever reported for the methanolysis of AB using nickel catalysts such as $NiCl_2$ (TOF = 2.9 min^{-1}) [25], Ni-Ni_3B (TOF = 5.0 min^{-1}) [29], Co-Ni-B (TOF = 10.0 min^{-1}) [29]. The high activity of preformed PVP-stabilized nickel(0) nanoparticles can be attributed to effective stabilization of nickel(0) nanoparticles by poly(N-vinyl-2-pyrrolidone) and the smaller particles size of nickel(0) nanoparticles found to be 3.0 ± 0.7 nm.

4. Conclusions

The main findings of this study plus their implications can be summarized as follows:

(1) Highly dispersed nickel(0) nanoparticles stabilized by PVP with average particle size of 3.0 ± 0.7 nm were reproducibly prepared from the reduction of nickel(II) 2-ethylhexanoate during the catalytic methanolysis of hydrazine borane in the presence of 2.0 mol PVP per mol of nickel. Polymer stabilized nickel(0) nanoparticles could be isolated from reaction solution by centrifugation and characterized by UV–vis spectroscopy, X-Ray photoelectron spectroscopy (XPS), transmission electron microscopy (TEM) and selected area electron diffraction (SAED) techniques.

(2) The main goal of the present study was to prepare an active nickel catalyst for hydrogen generation from the methanolysis of ammonia borane. Since ammonia borane cannot reduce the nickel(II) precursor, the stronger reducing agent hydrazine borane had to be used for the formation of nickel(0) nanoparticles. Thus, the nickel(0) nanoparticles were *in-situ* generated during the methanolysis of hydrazine borane and used to catalyze the methanolysis of both amine boranes.

(3) These *in-situ* formed PVP-stabilized nickel(0) nanoparticles exhibit high catalytic activity in hydrogen generation from the methanolysis of both hydrazine borane and ammonia borane at ambient temperature. The initial turnover frequency for the methanolysis of HB or AB catalyzed by PVP-stabilized nickel(0) nanoparticles was determined to be 35.6 min^{-1} or 12.1 min^{-1},

respectively, which are greater than the values reported in literature for the same reaction using different nickel catalysts.

(4) The kinetic studies reveal that methanolysis is first order with respect to catalyst concentration and zero order regarding to substrate concentration for the methanolysis of both HB and AB. The activation energy values determined for the catalytic methanolysis of HB and AB (63 ± 2 and 62 ± 2 kJ/mol, respectively) are close to each other.

(5) Performing carbon disulfide poisoning experiments showed that PVP-stabilized nickel(0) nanoparticles are kinetically competent catalyst and the catalytic methanolysis of HB and AB is heterogeneous.

(6) It is noteworthy that PVP-stabilized nickel(0) nanoparticles have higher total turnover number and turnover frequency in the methanolysis of hydrazine borane than that in the methanolysis of ammonia borane. Thus, they are more active and longer lived catalyst in the methanolysis of hydrazine borane than in the methanolysis of ammonia borane.

(7) Easy preparation, high stability, cost effectiveness and high catalytic performance of PVP-stabilized nickel(0) nanoparticles make them promising candidate to be exploited as catalyst for the portable hydrogen generation systems using hydrazine borane or ammonia borane as hydrogen storage material.

Acknowledgements

Partial support by Turkish Academy of Sciences and TUBITAK for a scholarship to DÖ is gratefully acknowledged.

References

[1] L. Schlapbach, A. Züttel, Nature 414 (2001) 353–358.
[2] S.M. Aceves, G.D. Berry, G.D. Rambach, Int. J. Hydrogen Energy 23 (1998) 583–591.
[3] Basic Research Needs For the Hydrogen Economy, Report of the Basic Energy Sciences Workshop on Hydrogen Production, Storage and Use, May 13–15, 2003, Office of Science, U.S. Department of Energy, http://science.energy.gov/~/media/bes/pdf/reports/files/nherpt.pdf
[4] A.D. Sutton, A.K. Burrell, D.A. Dixon, E.B. Garner, J.C. Gordon, T. Nakagawa, K.C. Ott, J.P. Robinson, M. Vasiliuet, Science 331 (2011) 1426–1429.
[5] C.W. Hamilton, R.T. Baker, A. Staubitz, I. Manners, Chem. Soc. Rev. 38 (2009) 279–293.
[6] H.W. Langmi, G.S. McGrady, Coord. Chem. Rev. 251 (2007) 925–935.
[7] A. Züttel, Mater. Today 6 (2003) 24–33.
[8] Annual Energy Outlook 2005 With Projections To 2025, Energy Information Administration, February 2005, www.eia.doe.gov/oiaf/aeo/pdf/0383(2005).pdf
[9] S. Hausdorf, F. Baitalow, G. Wolff, F. Mertens, Int. J. Hydrogen Energy 33 (2008) 608–614.
[10] H.B. Dai, L.L. Gao, Y. Liang, X.D. Kang, P. Wang, J. Power Sources 195 (2010) 307–312.
[11] T. Hügle, M.F. Kühnel, D. Lentz, J. Am. Chem. Soc. 131 (2009) 7444–7446.
[12] R. Moury, G. Moussa, U.B. Demirci, J. Hannauer, S. Bernard, E. Petit, A. van der Lee, P. Miele, Phys. Chem. Chem. Phys. 14 (2012) 1768–1777.
[13] J. Hannauer, U.B. Demirci, C. Geantet, J.M. Herrmann, P. Miele, Int. J. Hydrogen Energy 37 (2012) 10758–10767.
[14] G. Wolf, J. Baumann, F. Baitalow, F.P. Hoffman, Thermochim. Acta 343 (2000) 19–25.
[15] C.A. Jaska, K. Temple, A.J. Lough, I. Manners, J. Am. Chem. Soc. 125 (2003) 9424–9434.
[16] C.A. Jaska, I. Manners, J. Am. Chem. Soc. 126 (2004) 9776–9785.
[17] S. Akbayrak, S. Özkar, ACS Appl. Mater. Interfaces 4 (2012) 6302–6310.
[18] D. Sun, V. Mazumder, Ö. Metin, S. Sun, ACS Catal. 2 (2012) 1290–1295.
[19] S. Karahan, M. Zahmakıran, S. Özkar, Int. J. Hydrogen Energy 36 (2011) 4958–4966.
[20] M. Diwan, D. Hanna, A. Varma, Int. J. Hydrogen Energy 35 (2010) 577–584.
[21] M. Zahmakıran, S. Özkar, Top. Catal. 56 (2013) 1171–1183.
[22] D. Çelik, S. Karahan, M. Zahmakıran, S. Özkar, Int. J. Hydrogen Energy 37 (2012) 5143–5151.
[23] Ç. Çakanyıldırım, U.B. Demirci, T. Şener, Q. Xu, P. Miele, Int. J. Hydrogen Energy 37 (2012) 9722–9729.
[24] D.C. Zhong, K. Aranishi, A.K. Singh, U.B. Demirci, Q. Xu, Chem. Commun. 48 (2012) 11945–11947.
[25] P.V. Ramachandran, P.D. Gagare, Inorg. Chem. 46 (2007) 7810–7817.
[26] S.B. Kalidindi, U. Sanyal, B.P. Jagirdar, Phys. Chem. Chem. Phys. 10 (2008) 5870–5874.
[27] H. Erdogan, Ö. Metin, S. Özkar, Phys. Chem. Chem. Phys. 44 (2009) 10519–10525.
[28] H. Erdogan, Ö. Metin, S. Özkar, Catal. Today 170 (2011) 93–98.
[29] S.B. Kalidindi, A.A. Vernekar, B.R. Jagirdar, Phys. Chem. Chem. Phys. 11 (2009) 770–775.
[30] S. Çalışkan, M. Zahmakıran, S. Özkar, Appl. Catal. B: Environ. 93 (2010) 387–394.
[31] H.B. Dai, X.D. Kang, P. Wang, Int. J. Hydrogen Energy 35 (2010) 10317–10323.
[32] S. Karahan, M. Zahmakıran, S. Özkar, Dalton Trans. 41 (2012) 4912–4918.
[33] M. Zahmakıran, S. Özkar, Nanoscale 3 (2011) 3462–3481.
[34] M. Zahmakıran, S. Özkar, in: R. Luque, R.S. Varma (Eds.), Sustainable preparation of metal nanoparticles: methods and applications, RSC Publishing, London, 2013, pp. 34–66.
[35] Ö. Metin, S. Özkar, Int. J. Hydrogen Energy 36 (2011) 1424–1432.
[36] S.B. Kalidindi, M. Indirani, B.R. Jagirdar, Inorg. Chem. 47 (2008) 7424–7429.
[37] D. Özhava, A.M. Önal, S. Özkar, J. Electrochem. Soc., in review.
[38] F.C. Gunderloy, B. Spielvogel, R.W. Parry, Inorg. Synth. 9 (1967) 13–16.
[39] M.A. Watzky, R.G. Finke, J. Am. Chem. Soc. 119 (1997) 10382–10400.
[40] M.A. Watzky, R.G. Finke, Chem. Mater. 9 (1997) 3083–3095.
[41] J.A. Widegren, J.D. Aiken, S. Özkar, R.G. Finke, Chem. Mater. 13 (2001) 312–324.
[42] R. Takahashi, S. Sato, T. Sodesawa, H. Nishida, Phys. Chem. Chem. Phys. 4 (2002) 3800–3805.
[43] T. Umegaki, Q. Xu, Y. Kojima, J. Alloys Compd. 580 (2013) 313–316.
[44] J.A. Creighton, D.G. Eadon, J. Chem. Soc. Faraday Trans. 87 (1991) 3881–3891.
[45] G. Ertl, R. Hierl, H. Knozinger, N. Thiele, H.P. Urbach, Appl. Surf. Sci. 5 (1980) 49–64.
[46] A.N. Mansour, Surf. Sci. Spectra 3 (1994) 211–220.
[47] N.R. Gleason, F. Zaera, J. Catal. 169 (1997) 365–381.
[48] G. Schmid, Clusters and Colloids: From Theory to Applications, VCH Publishers, New York, 1994.
[49] S.O. Grim, L.J. Matienzo, W.E. Swartz, J. Am. Chem. Soc 94 (1972) 5116.
[50] A.N. Mansour, Surf. Sci. Spectra 3 (1994) 231–238.
[51] A.N. Mansour, Surf. Sci. Spectra 3 (1994) 221–230.
[52] A.K. Agegnehu, C.-J. Pan, J. Rick, J.-F. Lee, W.-N. Sub, B.-J. Hwang, J. Mater. Chem. 22 (2012) 13849–13854.
[53] C.H. Liu, B.H. Chen, C.L. Hsueh, J.R. Ku, F.K.J. Tsau, Catal. Appl. B 91 (2009) 368–379.
[54] S.C. Amendola, S.L. Sharp-Goldman, M.S. Janjua, M.T. Kelly, P.J. Petillo, M. Binder, J. Power Sources 85 (2000) 186–189.
[55] C.H. Liu, B.H. Chen, C.L. Hsueh, J.R. Ku, M.S. Jeng, F. Tsau, Int. J. Hydrogen Energy 34 (2009) 2153–2163.
[56] C.C. Su, M.C. Lu, S.L. Wang, Y.H. Huang, RSC Adv. 2 (2012) 2073–2079.
[57] K.J. Laidler, Chemical Kinetics, third ed., Harper & Row Publishers, New York, 1987.
[58] H. Eyring, J. Chem. Phys. 3 (1935) 107–115.
[59] S. Şencanlı, S. Karahan, S. Özkar, Int. J. Hydrogen Energy 38 (2013) 14693–14703.
[60] G. Cao, Y. Wang, Nanostructures & Nanomaterials: Synthesis, Properties and Applications, second ed., Imperial College Press, London, 2004.
[61] S. Özkar, R.G. Finke, J. Amer. Chem. Soc. 124 (2002) 5796–5810.
[62] B.J. Hornstein, J.D. Aiken, R.G. Finke, Inorg. Chem. 41 (2002) 1625–1638.
[63] M.N. Vargaftik, V.P. Zargorodnikov, I.P. Stolarov, I.I. Moiseev, D.I. Kochubey, V.A. Likholobov, A.L. Chuvilin, K.I. Zamaracv, J. Mol. Catal. 53 (1989) 315–348.